processes

MDPI

Article

Process Parameters and Heat-Treatment Optimization for Improving Microstructural and Mechanical Properties of AA6082-T651 Deposit on EN14B Plate Using Friction Surfacing Technique

Hemlata Jangid [1,*], Nirmal K. Singh [1] and Amlan Kar [1,2,*]

[1] Department of Mechanical Engineering, Indian Institute of Technology (Indian School of Mines), Dhanbad 826004, Jharkhand, India
[2] Arbegast Materials Processing and Joining Laboratory (AMP), South Dakota School of Mines and Technology, Rapid City, SD 57701, USA
* Correspondence: 21dr0060@mech.iitism.ac.in (H.J.); amlan.kar@sdsmt.edu (A.K.)

Abstract: Friction surfacing (FS) is increasingly recognized as an advanced technique for coating similar and dissimilar materials, enabling superior joint quality through plastic deformation and grain refinement. This study investigates the deposition of AA6082-T651 alloy on a medium-carbon steel EN14B substrate using FS, with process parameters optimized, and the effect of axial load, rotational speed, and traverse speed on coating integrity. The optimal sample was subjected to heat treatment (HT) at 550 °C for 24, 36, and 48 h to further enhance mechanical properties. Comprehensive microstructural and mechanical analyses were performed on both heat-treated and non-heat-treated samples using optical microscopy (OM), field emission scanning electron microscopy (FESEM) with energy-dispersive X-ray spectroscopy (EDS), X-ray diffraction (XRD), microhardness testing, and micro-tensile techniques. The optimized sample was processed with a 6 kN axial load, a rotational speed of 2700 rpm, and a traverse speed of 400 mm/min, and demonstrated superior bond quality and enhanced mechanical properties. The highest interfacial hardness values, 138 HV0.1 were achieved for the sample annealed for 48 h, under an axial load of 6 kN. Annealing for 48 h significantly improved atomic bonding at the aluminum–steel interface, confirmed by the formation of Fe_3Al intermetallic compounds detected via FESEM-EDS and XRD. These compounds were the primary reason for the enhancement in the mechanical properties of the FS deposit. Furthermore, the interrelationship between process and thermal parameters revealed that a peak temperature of 422 °C, heat input of 1.1 kJ/mm, and an axial load of 6 kN are critical for achieving optimal mechanical interlocking and superior coating quality. The findings highlight that optimized FS parameters and post-heat treatment are critical in achieving high-quality, durable coatings, with improved interfacial bonding and hardness, making the process suitable for structural applications.

Keywords: friction deposition; thermo-mechanical process; heat treatment; microstructure; mechanical properties

check for updates

Academic Editor: Chin-Hyung Lee

Received: 15 December 2024
Revised: 11 February 2025
Accepted: 18 February 2025
Published: 24 February 2025

Citation: Jangid, H.; Singh, N.K.; Kar, A. Process Parameters and Heat-Treatment Optimization for Improving Microstructural and Mechanical Properties of AA6082-T651 Deposit on EN14B Plate Using Friction Surfacing Technique. *Processes* **2025**, *13*, 637. https://doi.org/10.3390/pr13030637

Copyright: © 2025 by the authors. Licensee MDPI, Basel, Switzerland. This article is an open access article distributed under the terms and conditions of the Creative Commons Attribution (CC BY) license (https://creativecommons.org/licenses/by/4.0/).

1. Introduction

Coating technologies are increasingly adopted across industries to enhance productivity, extend product lifespan, and reduce manufacturing and maintenance costs. These advancements contribute significantly to reducing global material usage. Friction surfacing (FS), an evolution of the friction stir welding process, has emerged as a promising surface

modification technique, providing protection against corrosion and harsh environmental conditions. FS is a solid-state, thermo-mechanical coating process that relies on the plastic deformation of a metallic consumable rod. During FS, a rotating consumable rod is pressed against a substrate and traverses steadily, generating frictional heat sufficient to plasticize the rod material. This results in the deposition of a viscoelastic layer on the substrate, improving its mechanical, tribological, and corrosion properties [1].

Unlike conventional coating techniques, FS eliminates dilution, solidification cracks, internal stresses, and porosity. It is particularly advantageous for metallurgically incompatible materials, ensuring high adhesion between the coating and the substrate [2]. FS-treated surfaces retain the characteristics of the base material while enhancing microstructural properties, mechanical strength, and resistance to wear and corrosion. These attributes make FS a versatile solution for coating, joining, surface modification, composite material fabrication, and crack repair.

The quality of FS coatings depends heavily on process parameters such as axial force, rotational speed, and traverse speed, along with factors like ambient conditions and substrate pre-treatment. These parameters influence coating geometry (thickness, width, and length) and bonding strength [3]. Severe plastic deformation (SPD) during FS facilitates metallurgical bonding and grain refinement at the interface, improving coating strength and surface properties. In aluminum–steel systems, FS coatings enhance the efficiency substrate by preventing rust and corrosion while improving fatigue strength and tool life in challenging environments. Optimal process temperatures promote atomic diffusion between aluminum and steel, enhancing coating integrity. However, the limited solubility of aluminum in steel may lead to intermetallic compound (IMC) formation which, if not controlled, can compromise coating quality. Process parameter optimization, such as controlling rotational speed and consumable rod diameter, is critical to achieving suitable deposition temperatures and improving coating characteristics [4].

Depositing aluminum on steel through friction surfacing can enhance the efficiency of steel used in industries by eliminating rusting and corrosion, while also offering improved fatigue strength and tool life in harsh environments. Good atomic diffusion between Al and Fe will occur at elevated temperatures, and optimization of process parameters will enhance the deposit layer thickness and bond integrity. As the solubility of Al in Fe is low, it may cause microcracks and intermetallic compounds (IMCs) at the coating interface, which can be suppressed with increased process temperature and process parameters optimization [4]. By controlling the rotational speed and diameter of the consumable rod, an appropriate process temperature can be achieved, which further enhances the diffusion and bonding quality of the coating. In the experimentation, during the FS of AA 6351-T6 over a 6 mm thick steel plate, various diameters, like 8 mm, 12 mm, 16 mm, and 22 mm, were investigated. The 22 mm diameter consumable rod yielded excellent results as the temperature attained reached, on the advancing side, 451 °C and, on the retreating side, 375 °C [5]. Elemental diffusion of Fe into AA5083 was observed at the FSed interface. The metallic compound Fe_3Al was found, due to microstructure refinement at the deposition during the thermo-mechanical FSed coating process of the aluminum alloy 5083 on the DH36 steel plate. Microstructure and bonding strength improved at a lower travel speed, higher rotational speed, and axial load, while poor deposition quality was observed at increased travel speed, axial load, and lower rotational speed [6]. The use of pre-heat treatment during the single-layer friction-surfaced coating of AA6063 alloy over EN8 has led to many notable outcomes, including enhanced hardness at the interface, reduced flash generation, higher deposition rate, and better coating efficiency [7]. Furthermore, another attempt was made to enhance the heat transfer at the deformation phase. N_2 gas was supplied at the deposition area with a pressure of 4 bar, and its impact on FSed coating

metallurgy and bond strength was investigated. The forced convection process continued during and after the deposition phase, which could have prevented the formation of any intermetallic oxide compounds [8]. This work disclosed the influence of inductive heating of the substrate (EN8) during layer depositions of AISI 316 stainless steel using the FS technique; there was an increment in the consumption rate and deposition rate of 12.8% and 10.72%, respectively, as well as improved mechanical properties [9]. During the repair of alloy 718 using the solid-state friction surfacing method, the effect of the axial load was a more prominent factor in obtaining greater bond integrity; it was also seen that, at a lower rotational speed, more fine recrystallized grains were present in the coating compared to in high rotational speed deposits, which provides evidential proof of shear strength testing and the microstructural analysis of deposits [10]. In the deposition of Ti-6Al-4V, the importance of rotational speed in controlling coating geometry, grain refinement, and material flow behavior in the friction surfacing process was evident. At high rotational speed, increased process temperature leads to coarser grains; also, brittleness may be introduced in the FSed coating. When the process temperature reaches a steady state condition, the flash generation is averted, hence no change in temperature distribution due to different combinations of rotational speed and deposition speed [11]. The integrity of the coating was evaluated based on its quality, durability, and performance in critical applications such as wear and corrosion resistance. Also, the quality of the friction-surfaced (FSed) coating was assessed by evaluating its appearance, deposition efficiency (i.e., the uniformity and consistency of the coating), and tool efficiency (i.e., maximizing deposition while minimizing flash formation) [12]. Table 1 below summarizes the state of the art associated with the research carried out in this paper.

Table 1. Summary of previous research into solid-state coating and key findings.

Reference	Material Used	Main Focus	Key Findings
Reddy et al. (2011) [2]	FS of AA2124SiCp MMC consumable onto Ti6Al4V alloy substrate	Adequate bonding between AA2124SiCp MMC and Ti6Al4V alloy revealed by interdiffusion	Significant improvement in wear resistance caused by the presence of hard carbide particles in the Al alloy matrix, and Ti_3Al proves the diffusion.
Yu et al. (2022) [4]	FSSW of AA6061 alloy and Q235 steel	Microstructure and interface evolution	Fe-rich IMC at Al–steel interface, which leads to an improvement in mechanical properties.
Badheka and Badheka (2017) [5]	Friction surfacing of aluminum on steel	Effects of consumable rod diameter	Peak temperature advancing side (421 °C) is higher than retreating side (375 °C).
Li et al. (2019) [6]	Friction surfacing of aluminum alloy 5083 on DH36 steel plate	Effect of process parameter on coating quality	IMC FeAl3 was produced at the interface.
Sahoo et al. (2022) [7]	Al 6063 over EN8 steel FS	Pre heat-treatment applied	Enhanced hardness and bonding strength.
Kumar Sahoo et al. (2023) [8]	Effect of forced convection in FS	N_2 gas at 4 bar	Reduced oxide formation, improved bond strength.
Sahoo et al. (2020) [9]	Inductive heating during FS	Rotational speed, axial load	12.8% higher deposition rate, improved mechanical properties.
Govardhan et al. (2012) [13]	FS of stainless steel on low-carbon steel	Heat input control	Improved coating integrity, optimized heat input required.
Pereira et al. (2014) [14]	Multi-layer coatings of AISI 1024, AISI 1045 and AISI H13 over mild steel	Phase transformation	Formation of bainitic and martensitic microstructures in coating results in improved hardness and wear resistance.
Janakiraman et al. (2012) [15]	Composite surface formation via FS on Al–steel	Axial load, rotational speed	FS produced strong interfacial bonding.

Table 1. *Cont.*

Reference	Material Used	Main Focus	Key Findings
Yang et al. (2018) [16]	Interfacial bonding in Al–steel FS	Heat treatment effects	IMC formation critical to bonding strength.
Manesh et al. (2003) [17]	Annealing effects on Al-clad steel	Annealing	Enhanced ductility and bonding strength.
Martins et al. (2023) [18]	Fe aluminide coatings via FS	Heat treatment	Fe-rich IMCs formed after post-treatment.
Zhang T et al. (2023) [19]	FSW QP980 steel and AA6061	Intermetallic compounds (IMCs) play an important role in the welding quality of steel and aluminum	The interfacial bonding strength of IMCs with Fe and Al matrices and their effect on joint efficiency.
Jiang B et al. (2025) [20]	FSAM-formed 6082-T6 aluminum alloy underwent heat treatment	The influence of heat treatment on the microstructure and mechanical properties	Heat treatment increased hardness and caused abnormal growth of equiaxed grains in the HTAZ sample.

Despite advancements, significant knowledge gaps remain regarding parameter optimization for diverse material combinations. The correlation between axial force, rotational speed, and traverse speed requires further investigation to establish standardized guidelines for coating geometry and properties. Detailed microstructural analysis under varying thermal cycles and heat treatment conditions is essential to improve the mechanical and tribological properties of FS coatings in real-world applications. Also, the area related to the post-heat treatment of a dissimilar joint or FS still needs exploration.

This study aims to deposit a reinforced layer of AA6082-T651 alloy on medium-carbon steel EN14B, using the friction stir surfacing (FSS) process. The primary objective is to enhance the microstructural and mechanical properties of the substrate, ensuring optimal performance in various manufacturing sectors. The effects of heat treatment at 550 °C for 24, 36, and 48 h on the microstructural and mechanical behavior of FSS coatings were systematically evaluated. Additionally, the influence of individual process parameters, including axial load, rotational speed, and travel speed, on microhardness and microtensile strength was assessed. This study further explores the relationship between process parameters and heat treatment conditions to optimize FS coating quality.

2. Materials and Experimentation

2.1. Materials and Methods

The friction stir coating (FSC) of AA6082-T651 aluminum alloy on medium-carbon manganese steel EN14B was conducted using a horizontal friction stir machine (make: ETA Technologies, Bengaluru, India; model: WS0002) operating in force-controlled mode, as illustrated schematically in Figure 1a. The FSW machine setup and consumable tool after FS deposition are also shown in Figures 1b and 1c, respectively. A consumable tool with a diameter of 20 mm was employed to deposit an average coating thickness of 1.20 ± 0.25 mm on a 5.5 mm thick EN14B substrate. The chemical compositions of the consumable alloy and substrate material are detailed in Tables 2 and 3, respectively.

Before deposition, the EN14B steel plates were ground to enhance surface roughness, improving adhesion between the coating and substrate. Both the steel substrate and aluminum consumable rod were cleaned with acetone and treated with WD-40 spray to eliminate contaminants and prevent oxidation during FSC. AA6082-T651 rods were prepared with dimensions of 52 ± 0.50 mm in length, 28.44 ± 0.60 mm in width, and 1.20 ± 0.25 mm in thickness.

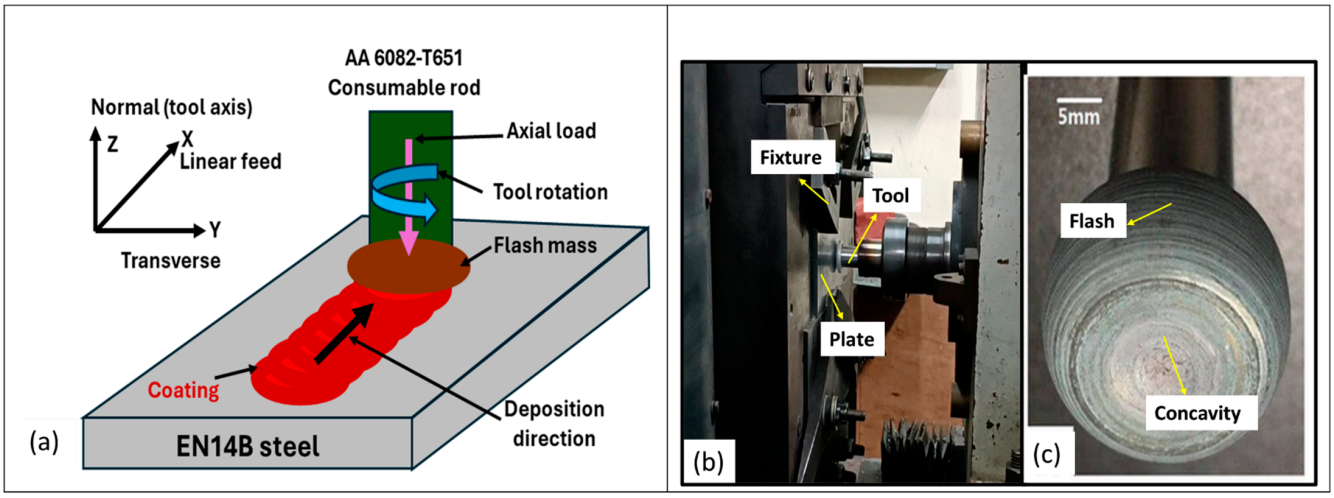


Figure 1. (**a**) Schematic diagram of the friction surfacing with process parameters, (**b**) FSW machine setup, and (**c**) consumable tool after FS deposition.

Table 2. Chemical composition of AA6082-T651 aluminum alloy (Al-Mg-Si alloy).

Alloy	Proportion of the Constituting Elements (wt.%)						
AA6082-T651	Mg	Mn	Fe	Si	Cu	Others (Cr + Ni + Zn +Ti)	Al
	1.10	0.60	0.25	0.90	0.07	0.40	Bal.

Table 3. Chemical composition of EN14B (medium-carbon manganese steel).

Alloy	Proportion of the Constituting Elements (wt.%)								
EN14B	C	Mn	P	Si	S	Cr	Mo	Ni	Fe
	0.35–0.45%	0.80–1.20%	0.040% max	0.20–0.50%	0.040% max	0.25% max	0.10% max	0.40% max	Bal.

2.2. Design of Experiment and Optimization Procedure

The experimental design was estimated using Taguchi's L9 orthogonal array (three factors, three levels) for performing the experiments. Also, the effects of axial load, rotational speed, and traverse speed on coating integrity were seen. Factor levels were assigned as (−1) for low, (0) for medium, and (+1) for high, as summarized in Table 4.

Table 4. FS process parameters and response outcomes.

Sample No.	Axial Load (KN)	Rotational Speed (RPM)	Traverse Speed (mm/min)	Length (mm)	Thickness (mm)	Width (mm)
S1	4(−1)	2300(−1)	200(−1)	50 ± 0.45	2.67 ± 0.10	25 ± 0.20
S2	4(−1)	2500(0)	400(0)	52 ± 0.30	2.25 ± 0.12	24 ± 0.10
S3	4(−1)	2700(+1)	600(+1)	65 ± 0.65	2.00 ± 0.18	23 ± 0.40
S4	5(0)	2300(−1)	400(0)	51 ± 0.55	2.15 ± 0.15	30 ± 0.30
S5	5(0)	2500(0)	600(+1)	53 ± 0.40	1.00 ± 0.20	28 ± 0.45
S6	5(0)	2700(+1)	200(−1)	40 ± 0.60	2.07 ± 0.18	29 ± 0.20
S7	6(+1)	2300(−1)	600(+1)	65 ± 0.10	1.25 ± 0.15	31 ± 0.35
S8	6(+1)	2500(0)	200(−1)	38 ± 0.35	1.35 ± 0.10	32 ± 0.10
S9	6(+1)	2700(+1)	400(0)	56 ± 0.25	0.90 ± 0.28	34 ± 0.15

Preliminary trials revealed that axial loads below 4 kN and rotational speeds below 2300 RPM were insufficient for effective bonding, resulting in peeling or poor coating quality. The optimized samples, S9, showed the best bonding quality and were subjected to detailed microstructural and mechanical analyses.

2.3. Heat Treatment Procedure

After the deposition of AA6082 T-651 on the EN14B steel substrate, heat treatment (HT) was conducted to further improve the bond quality of optimally coated samples. The heat treatment involved annealing the friction-surfaced specimens at a temperature of 550 °C for different time durations (24, 36, and 48 h). These durations were based on prior studies, experimental trials, and phase transformation data, which suggest significant atomic diffusion and IMC formation at the 550 °C temperature, which promotes diffusion bonding and the formation of Fe-rich IMCs [21,22]. The heat treatment was carried out in a muffle furnace, ensuring a consistent temperature throughout the process. Heat treatment was conducted with a heating rate of 4 °C/min up to 550 °C, followed by controlled cooling at 2 °C/min to 300 °C. The specimens were then allowed to cool naturally to room temperature after the specified duration of annealing.

2.4. Characterization Techniques

Microstructural characterization of non-heat-treated (NHT) and heat-treated (HT) samples was performed using optical microscopy, field-emission scanning electron microscopy (FE-SEM) equipped with energy-dispersive X-ray spectroscopy (EDS), and a Rigaku SmartLab X-ray diffraction (XRD), employing Cu Kα radiation at 3 kW, with a step size of 2° and a dwell time of 5 s. Samples (5 × 3 mm) were embedded in resin, mechanically ground (600–2000 grit), and polished with 0.1 µm diamond paste. Etchants included Nital for steel and a NaOH solution followed by Weck's reagent for aluminum.

Mechanical properties were assessed using a Vickers microhardness tester (Model HM220) with a 0.1 kgf load and a 15 s dwell time, and a ZwickRoell Model-Kappa, Mini creep testing machine, Austria (5 kN capacity) for micro-tensile tests, determining yield tensile strength (YTS) and ultimate tensile strength (UTS). The relationship between process parameters and heat input was examined to optimize deposition quality and analyze changes in microstructural and mechanical characteristics.

2.5. Mathematical Representation of Relation Between Process and Thermal Parameters

The friction surfacing (FS) process is highly dependent on process parameters such as axial load, rotational speed, and traverse speed, which directly affect heat input and peak temperature. There is no model still used for the correlation between process and thermal parameters. So, in this study, we used the equation proposed in FSW, which serves as a comparative tool for assessing heat input rather than as a precise temperature predictor. The relationships between torque, process parameters, weld power, and heat input are described in the following empirical equations:

$$\text{Weld power (p)} = \frac{\mathbf{2\pi\omega M}}{\mathbf{60}}\text{watts} \tag{1}$$

$$\text{Heat input (H.I)} = \frac{\boldsymbol{p}}{\boldsymbol{v}}\ \text{joules/mm} \tag{2}$$

where $\boldsymbol{\omega}$ is the tool rotational speed in RPM, $\boldsymbol{M}$ is torque in N·m, and $\boldsymbol{v}$ is the tool traverse speed in m/s. Weld power and heat input are measured in watts and joules, respectively.

$$\mathrm{T_{peak}} = \mathrm{T_{initial}} + \frac{\boldsymbol{P(friction)}}{\boldsymbol{m} \times \boldsymbol{Cp}} \tag{3}$$

Here, $\mathrm{T_{initial}}$ is the room temperature of the consumable rod, $\boldsymbol{P_{(friction)}}$ is the power generated due to friction (which can be calculated using the axial load and the tangential speed of the rotating tool), $\boldsymbol{C_p}$ is the specific heat capacity of the material, and $\boldsymbol{m}$ is the mass of the material being heated.

3. Results and Discussion

3.1. Coating Integrity and Quality

The appearance of the Al-deposited steel coatings is shown in Figure 2. Visual inspection and chisel–hammer tests were performed to assess the primary adhesion strength of the coating [13]. To characterize the coating geometry, measurements of length, width, and thickness were taken at three different points using digital vernier calipers. The average values of these dimensions are presented in Table 4. The figures illustrate the top view of a few samples.

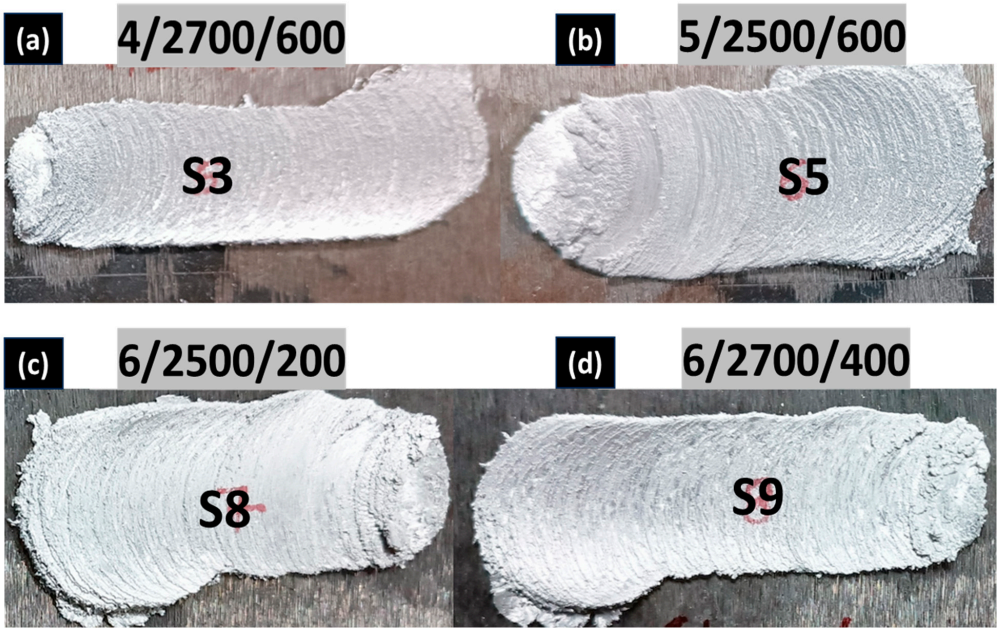


Figure 2. FSed deposition of AA6082 on EN14B at different processing conditions. Axial load/rotation speed/traverse speed are shown in each image.

The results revealed insufficient bonding between the substrate and the consumable material at a 4 kN axial load, particularly at higher traverse speeds of 600 mm/min in Sample S3. In this case, the increased traverse speed led to reduced contact time between the substrate and the consumable, resulting in a narrower deposited coating, as seen in Figure 2a. In contrast, samples produced with higher axial loads of 5 kN and 6 kN (e.g., Samples S5, S8, and S9) exhibited increased deposition widths, indicating stronger bonding. Optimal coating configurations were achieved in Samples S7 and S9, where both lower (2300 rpm) and higher (2700 rpm) rotational speeds were combined with a high axial load of 6 kN. Sample S7, produced at 2300 rpm, demonstrated intermediate bonding strength, while Sample S9 exhibited the highest bonding strength.

Across the trials, including Samples S5, S6, S7, S8, and S9, it was observed that higher traverse speeds resulted in thinner coatings due to reduced time for effective bonding and material spreading. Thicker coatings were generally achieved at lower traverse speeds, which allowed more time for material deposition. However, it is important to note that thicker coatings do not necessarily correlate with higher quality, as evidenced by Sample S3 which, despite having a thickness of 2.00 $\pm$ 0.18 mm, exhibited weaker bonding due to insufficient time for effective metallurgical bonding. The correlation between coating thickness and bond strength is based on well-established principles of metallurgical bonding in friction surfacing. While thicker coatings often result from higher material deposition, bond strength primarily depends on interfacial bonding quality, which is influenced by factors like heat generation, plastic deformation, and diffusion [23,24].

Wider coatings were achieved at higher rotational speeds, as these increased the heat input, facilitating better material spreading. On the contrary, higher traverse speeds resulted in narrower coatings, as the reduced time available for the cladding material to spread laterally led to narrower deposition tracks. The influence of these processing parameters on bonding strength will be further discussed in subsequent sections of this study.

As verified by the above experiments, the significant differences in the thermal and mechanical properties of aluminum and steel present challenges in optimizing process parameters, controlling flash formation, and ensuring deposition efficiency during the FS of aluminum on steel. Both axial load, rotational speed, and traverse speed play crucial roles in improving the bond strength of FS coatings [14]. A higher axial load enhances interlocking at the interface by inducing greater plastic deformation, which strengthens the mechanical interlocking. On the other hand, an increased traverse speed reduces heat generation, leading to defect formation and, therefore, compromising the integrity of the coating. In addition, higher rotational speeds enable optimal interlocking due to increased deformation, generating more heat and enabling the formation of a thin intermetallic compound (IMC) layer. Furthermore, elevated heat and material softening during deposition further contribute to the improved quality of the interface. To achieve optimal coating quality and integrity, a combination of a higher axial load and higher rotational speed with traverse speed is recommended, as outlined in Table 4 and Figure 3 [15].

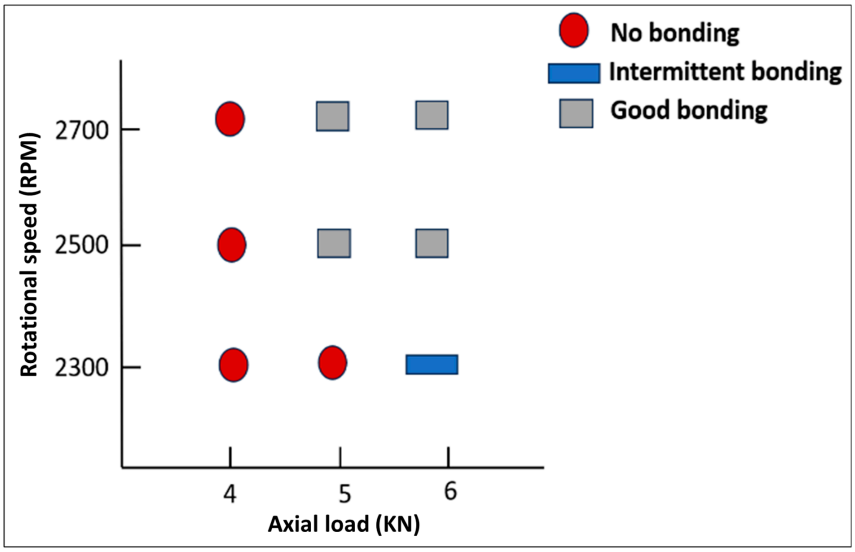


Figure 3. Influence of axial load and rotational speed on the bond quality, showing a window of good and no bonding.

3.2. Microstructural Characterization

3.2.1. Non-Heat-Treated Samples

Microstructural analysis of the friction-surfaced (FSed) aluminum coating on the steel substrate revealed that bonding occurs through a combination of mechanical interlocking and metallurgical bonding. These mechanisms are facilitated by the intense frictional heat and pressure generated during the friction surfacing process [16]. In Sample S9, mechanical interlocking is evident at the interface, with a fragmented and wavy structure, as shown in Figure 4a. The metallurgical bonding is indicated by the thickness of the interface layer, which reflects the formation of atomic bonds between the aluminum and steel. Figure 4b presents a macrograph of the cross-section of Sample S9, taken with an optical microscope (DG Victory-Dewinter) at magnification: ×200. The image clearly demonstrates mechanical interlocking, with rough surface features and a wavy interfacial structure formed during the FS process. As the rotating tool traverses the substrate, frictional heat softens the

material at the interface, promoting metallurgical bonding and ensuring the integrity of the coated layer. During plastic deformation, mechanical interlocking predominates, followed by elemental diffusion during the cooling cycle, leading to metallurgical bonding.

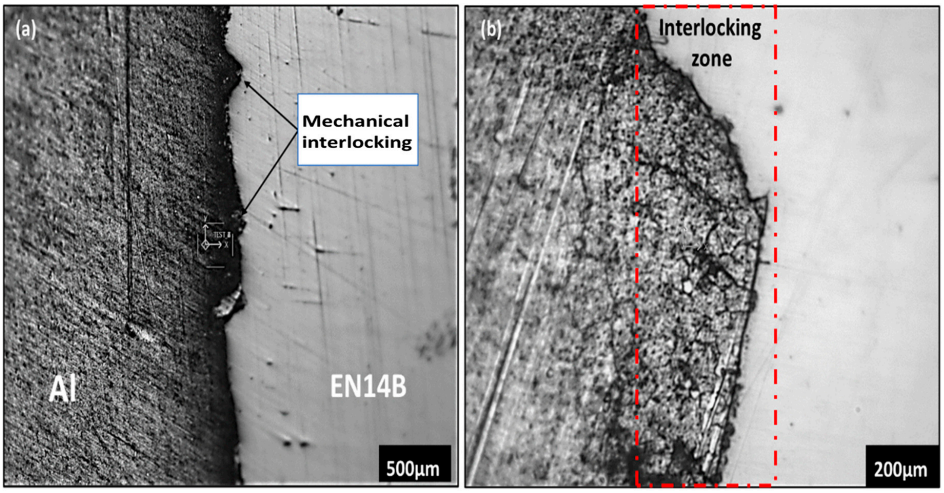


Figure 4. (a) Al–steel coating transition area for Sample S9 and (**b**) magnified view of the cross-section of Sample S9.

3.2.2. Heat-Treated Samples and Comparative Analysis

Microstructural analyses were performed on various regions, including the aluminum coating, base plate, and aluminum–steel interface, for both non-heat-treated (NHT) and heat-treated (HT) FSed coatings. Figure 5a,b show optical micrographs of the NHT and HT aluminum coatings of Sample S9, respectively. The images reveal significant grain refinement in the heat-treated sample due to the thermal effects of the friction surfacing process. Grain refinement was more pronounced in the heat-treated sample compared to the NHT sample. Sample S9 was selected for detailed analysis due to its anticipated superior bonding quality, which was expected to minimize defect formation, as suggested by the processing parameters in Figure 3. Grain size measurements were conducted using ImageJ software version 1.52e. The average grain size in the NHT aluminum deposit was 9.09 ± 0.49 µm while, in the HT aluminum deposit, it was reduced to 6.09 ± 0.25 µm. These microstructural differences are primarily due to the varying strain and thermal gradients induced during the process. The reduction in grain size is attributed to dynamic recrystallization, which is induced by severe plastic deformation [17,25] and static recrystallization being active during the cooling cycle of the FS process.

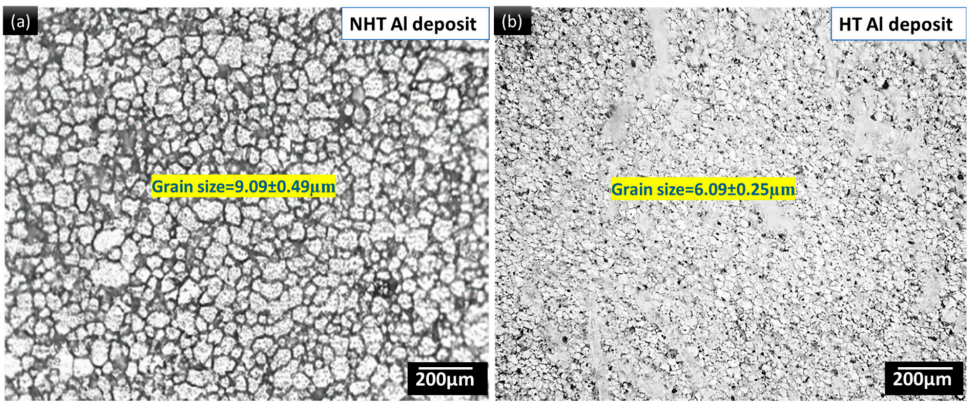


Figure 5. Optical micrograph associated with (**a**) NHT and (**b**) HT aluminum deposits during FS of the optimized sample (S9).

High-magnification FESEM images of the FSed coating interface were also analyzed to assess bond integrity under different applied loads (5 kN (S5) and 6 kN (S9)), as shown in Figures 6a and 6b, respectively. These images reveal the coating thickness, interface width (transition zone thickness), and any cracks present at the coating interface. Cracks were observed in the FSed deposit, attributed to low plasticity, uneven thermal expansion and contraction of the materials, and rapid cooling. The FESEM image of the sample with optimum FS process conditions (S9), shown in Figure 6c with higher magnification, highlights the single-layer deposition mechanism and consolidation to the base material. The wavy and irregular interface between the aluminum coating and steel substrate, caused by severe plastic deformation and mechanical mixing during friction surfacing, confirms mechanical interlocking [26].

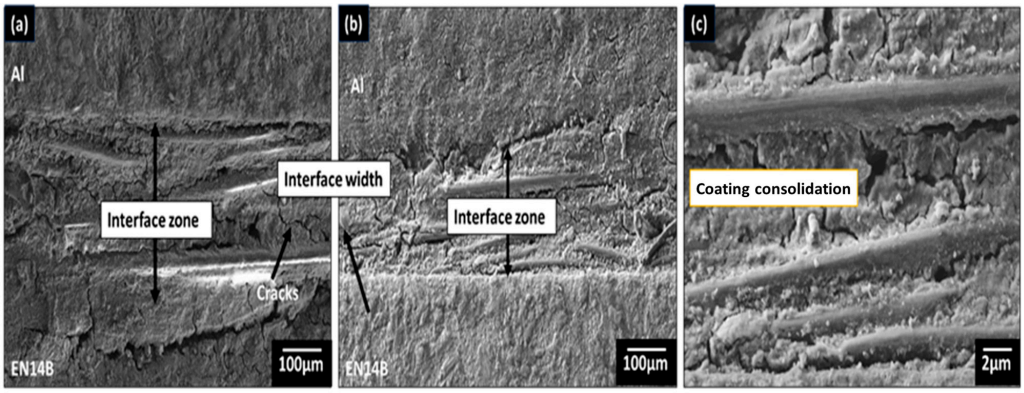


Figure 6. FSed coating of NHT samples obtained at (**a**) 5 KN (S5), (**b**) 6 KN (S9), and (**c**) magnified FESEM image of optimized coating sample.

Figure 7a–c present FESEM images of heat-treated samples, subjected to heat treatment at 550 °C for 24, 36, and 48 h, respectively. Post-heat treatment and cooling to room temperature, cracks were observed near the interface zone in Samples S9 (24 h) and S9 (36 h), likely due to the mismatch in thermal properties between aluminum and steel. However, in Sample S9 (48 h) (Figure 7c), Al-rich and Fe-rich intermetallic compounds (IMCs) were detected at the interface following 48 h of annealing. The magnified view in Figure 7d demonstrates stable interface bonding achieved after annealing at 550 °C for 48 h, where the formation of IMCs such as Al_3Fe and Fe_3Al enhances bonding integrity.

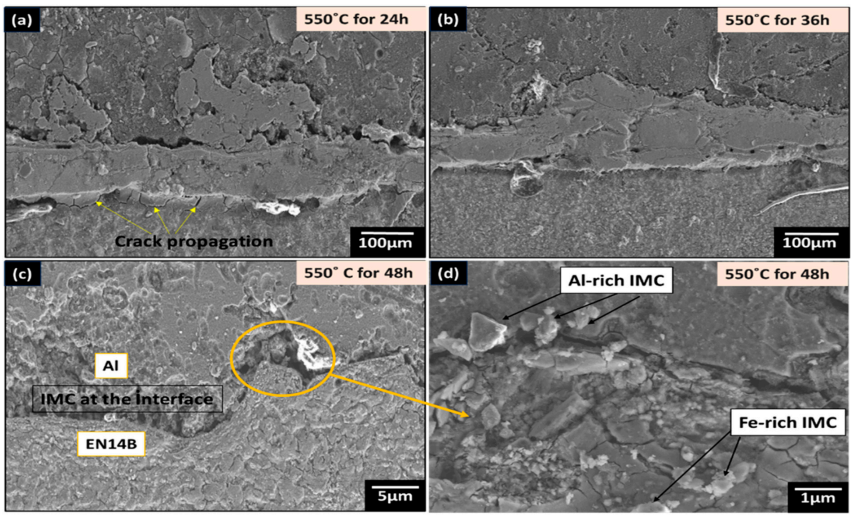


Figure 7. FESEM images of heat-treated (HT) samples for (**a**) 24 h, (**b**) 36 h, (**c**) 48 h, and (**d**) a magnified image of HT for 48 h.

Energy dispersive spectroscopy (EDS) analysis of the Al–steel interface in friction surfacing samples subjected to heat treatment for 24 h, 36 h, and 48 h is shown in Figure 8b–d, respectively. The EDS spectra, particularly Spectrum 2, highlight significant morphological changes at the Al–steel interface. Figure 8c,d show that heat treatment at 550 °C for 36 h and 48 h promotes enhanced solid solubility of aluminum into iron, leading to the formation of a diffusion layer/interface. It was observed that the aluminum percentage decreased with an increase in heat treatment (HT) duration. The reduced aluminum content at the Al/interface region (Spectrum 2) can be attributed to the progressive formation of intermetallic compounds (IMCs) as the HT duration increased. This mutual diffusion of Fe and Al atoms alters the lattice structure, transforming the bond from a diffusion-based bond to a stronger metallurgical (atomic) bond, thereby improving bonding strength [17,18,20].

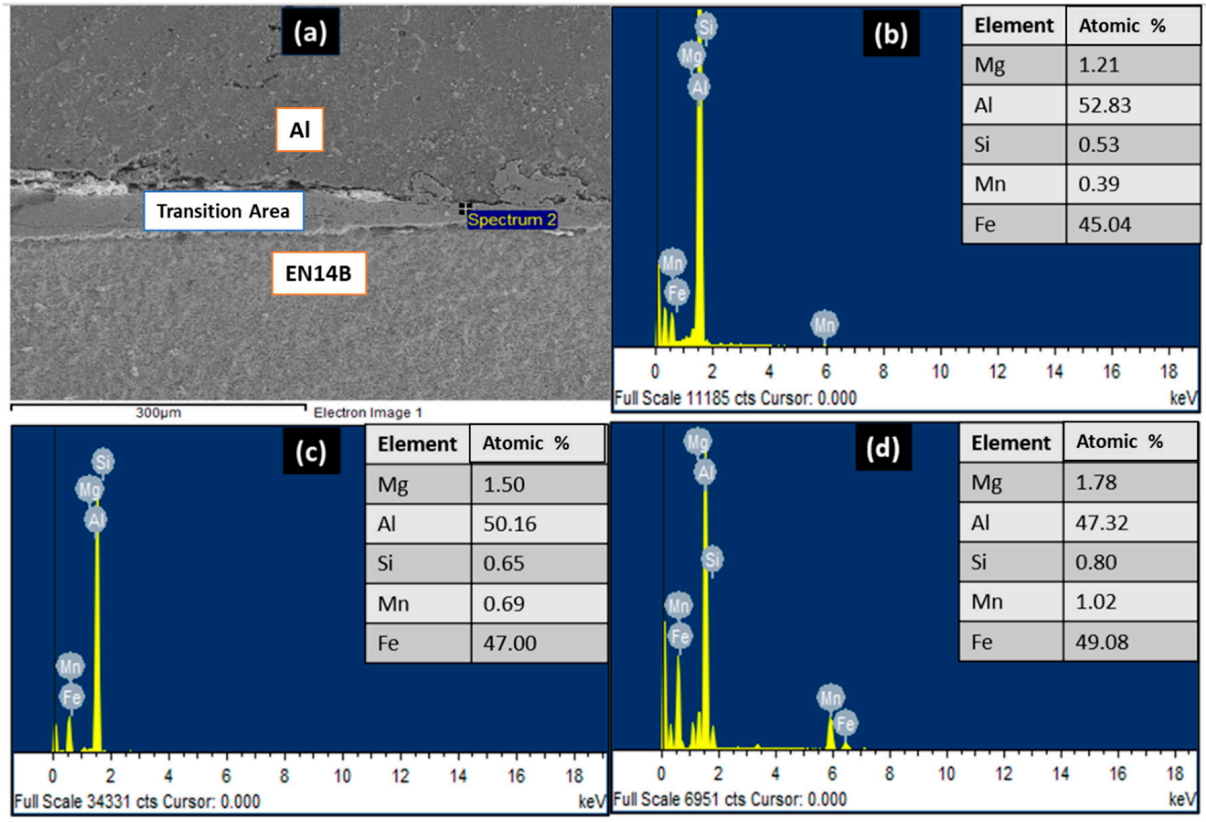


Figure 8. (**a**) Al–steel interface at Spectrum 2, and (**b**–**d**) depict the EDS information of Samples S9 at 24 h, 36 h, and 48 h at the interface.

Figure 9 shows the EDS data for the heat-affected zone (HAZ) on the steel side, specifically at Spectrum 3. The data reveal that aluminum diffusion into iron was higher in Sample S9 (36 h) than in Sample S9 (24 h), as shown in Figure 9b,c. Additionally, in Sample S9 (48 h), the diffusion of aluminum into iron was further enhanced, as seen in Figure 9d. The atomic percentages of Fe (62.99%) and Al (18.00%) in Spectrum 3 indicate the presence of the Fe_3Al intermetallic phase in the HAZ of the steel side. It was observed that the percentage of aluminum decreased with an increase in heat treatment (HT) duration. The lower percentage of iron at the interface/Fe side (Spectrum 3) with increasing HT duration indicates higher diffusion of Fe into the Al region. This diffusion ultimately facilitates the formation of intermetallic compounds (IMCs), provided there is sufficient activation energy to drive the reaction.

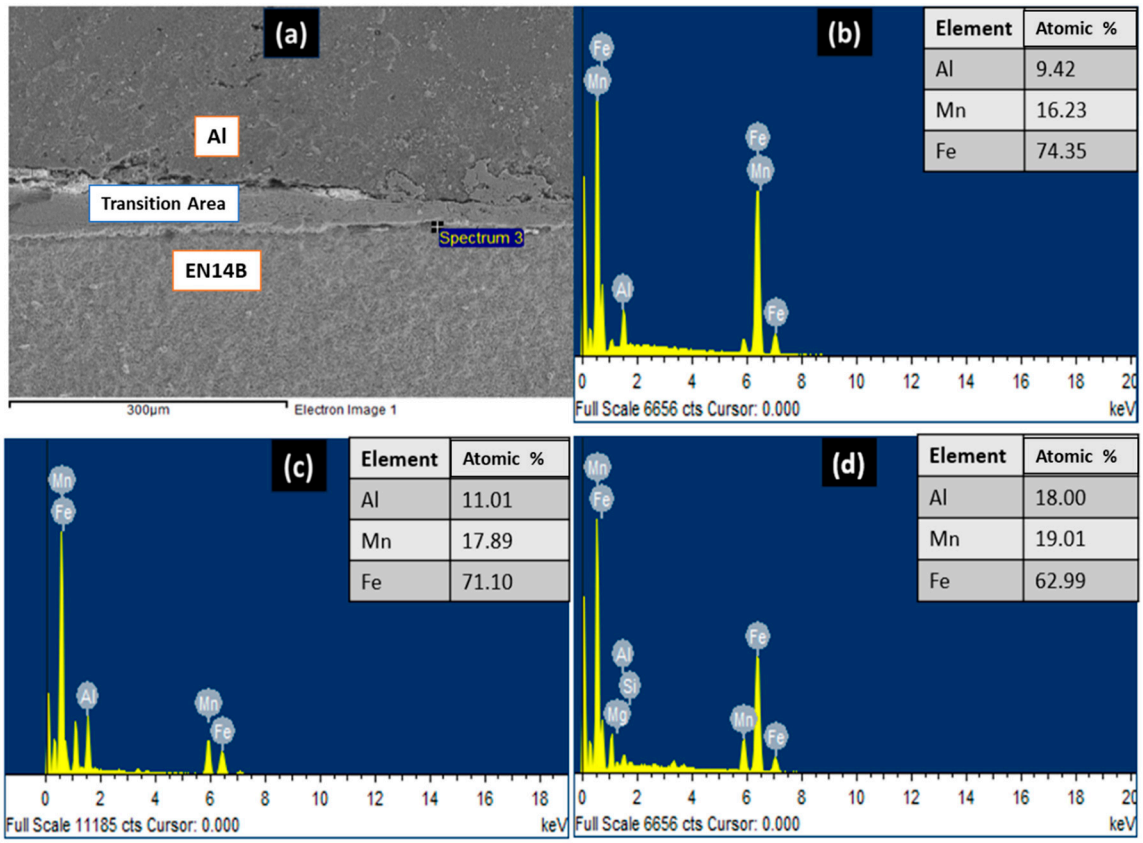


Figure 9. (**a**) Al–steel interface at Spectrum 3, and (**b**–**d**) depict the EDS information of Sample S9 at 24 h, 36 h, and 48 h at the interface.

3.3. Phase Analysis

The specimen, consisting of AA6082-T651 deposited over EN14B steel, was characterized for phase analysis with XRD data. The X-ray diffraction (XRD) phase map for both heat-treated and non-heat-treated samples is shown in Figure 10.

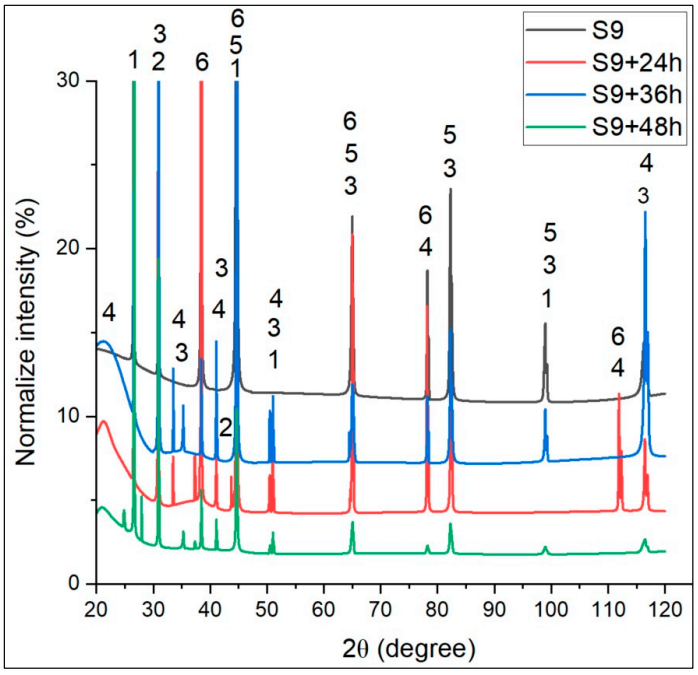


Figure 10. XRD pattern analysis of EN14B steel coated with aluminum AA6082 using the FSed method.

Phase analysis revealed significant diffusion activity between aluminum and steel at the interface following the heat treatment of Sample S9 at 550 °C for 24, 36, and 48 h. The XRD patterns for these heat-treated samples are presented in Figure 10. The diffractograms indicate the presence of several intermetallic compounds, as listed in Table 5, including Fe_3Al, $Fe_{0.90}Mg_{0.10}$, $Al_{0.6}Cr_{0.5}Fe_1$, $Al_{1.915}Fe_{0.082}Mg_{0.989}O_4$, α-Fe, and Al. These compounds form due to the low process temperature and the shorter contact time of the consumable rod with the steel substrate during friction surfacing.

Table 5. Intermetallic compounds along with their plane in XRD analysis.

S.No	Compounds
1	Fe_3Al
2	$Fe_{0.90}Mg_{0.10}$
3	$Al_{0.5}Cr_{0.5}Fe_1$
4	$Al_{1.915}Fe_{0.082}Mg_{0.989}O_4$
5	α-Fe
6	Al

In the untreated S9 sample, the dominant phases identified were Fe_3Al (peak 1) and $Al_{0.6}Cr_{0.5}Fe_1$ (peak 3), along with minor contributions from $Fe_{0.90}Mg_{0.10}$ (peak 2) and α-Fe (peak 5). Following heat treatment at 550 °C for 24 h, a noticeable increase in the intensity of peaks corresponding to $Al_{1.915}Fe_{0.082}Mg_{0.989}O_4$ (peak 4) and Al (peak 6) was observed, indicating the formation of these compounds during the heat treatment process.

As the treatment duration increased to 36 and 48 h, further growth of these intermetallic compounds was observed, with peaks 4 and 6 becoming more pronounced. This indicates enhanced phase formation and crystallinity with prolonged heat treatment. Notably, the α-Fe phase (peak 5) exhibited a gradual decrease in intensity as the heat treatment time increased, suggesting a reduction in the amount of this phase as it transformed into more stable intermetallic compounds at higher temperatures.

The S9 sample treated for 48 h exhibited Fe-rich intermetallic compounds such as Fe_3Al and $Al_{0.5}Cr_{0.5}Fe_1$ due to the extended annealing period. This phase evolution is beneficial for coating performance, enhancing the bonding strength and hardness [25]. In contrast, without heat treatment, only Al-rich intermetallics were observed. The diffusion of Al into Fe during heat treatment facilitated the formation of intermetallics with a higher Fe content, such as $Al_{0.5}Cr_{0.5}Fe_1$. This increase in Fe-rich intermetallics significantly contributed to the improvement in bonding strength, with hardness values reaching up to 900 HV [18]. While it is true that IMCs can enhance hardness due to their inherent rigidity, excessive formation can indeed lead to brittleness, compromising overall toughness and impact resistance at the interface Therefore, a balance between beneficial and detrimental IMC formation is crucial [19,27].

3.4. Mechanical Characterization

3.4.1. Microhardness Test

In this study, the microhardness of friction-surfaced (FSed) coated samples was analyzed at the aluminum deposit, the Al-steel interface, and the heat-affected zone (HAZ) of the steel, as shown in Figure 11. The average microhardness values for steel (EN14B) and the consumable (AA6082 T-651) were 233 HV0.1 and 89 HV0.1, respectively. The hardness at the Al–steel interface increased by 24.18% in Sample S9 after 48 h of heat treatment compared to the untreated S9 sample. The maximum hardness values at the Al–steel interface was 138 HV0.1, 132 HV0.1, and 124 HV0.1 in the heat-treated Sample S9 for 48 h, 36 h, and 24 h, respectively. In the untreated sample, the hardness at the Al–steel interface was 118 ± 5 HV0.1, which can be attributed to the thermo-mechanical

deformation, leading to significant microstructural refinement, elemental diffusion, and IMC formation at the interface. The increased hardness in the HAZ is primarily attributed to grain refinement resulting from thermal cycling during friction surfacing. Martensite formation is unlikely at the observed temperatures (~550 °C), as they are below the critical transformation temperature for the steel used. This refinement contributes to an increase in the hardness of the deposited layer.

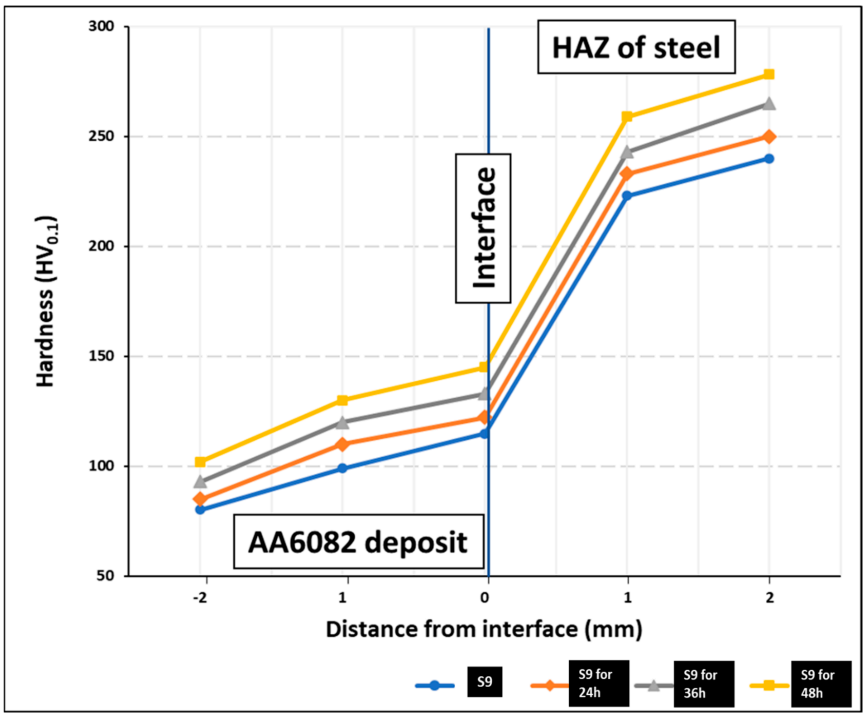


Figure 11. Microhardness of AA6082-coated FSed samples across the interface.

A decreasing hardness trend (98 ± 8 HV0.1) was observed in the deposited layer towards the height of the coating, due to variations in thermal exposure and grain refinement. The hardness of the as-coated deposited layers was significantly lower (85 ± 8 HV0.1) than that of the consumable rod (89 ± 4 HV0.1). The effects of different process parameters, such as axial load, rotational speed, and travel speed, on the microhardness are shown in Figure 12. This indicates that both axial load and traverse speed have a direct impact on the hardness of the FSed deposit. Additionally, an increase in hardness was observed in the heat-affected zone of the steel, with a 17.16% increase attributed to grain refinement and IMC formation during the FS process, which enhances the hardness of material [28,29].

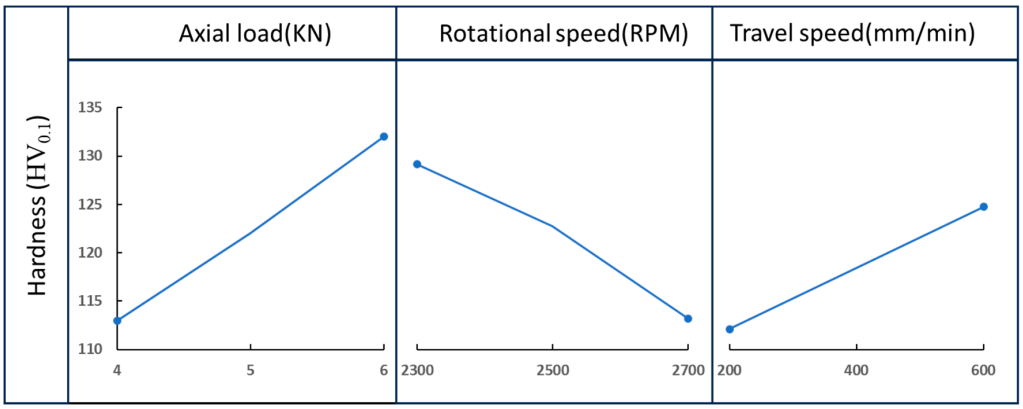


Figure 12. Influence of process parameters on the microhardness of the FSed coating.

3.4.2. Micro-Tensile Test

Tensile testing was performed to assess the reliability and performance of the FSed coated samples for structural applications. A typical tensile test specimen, containing both the coating and the deposited material, was cut according to ASTM E8 [30] dimensions using wire-cut EDM. The samples were extracted perpendicular to the interface plane, with approximately 50% of the gauge length within the deposited layer. The displacement rate was 0.50 mm/min during tensile testing.

The individual effects of process parameters such as axial load, rotational speed, and travel speed on the ultimate tensile strength (UTS) are shown in Figure 13. The findings indicate that the maximum UTS values were achieved with process parameters of 6 kN, 2700 RPM, and 400 mm/min. The results of the tensile test of the AA6082-coated EN14B steel specimen showing comparative variation in the tensile strength of base Al and deposited Al at different directions (Specimen 1 along longitudinal and Specimen 2 along transverse directions) are presented in Figure 14. Specimen 1 was cut from the deposited material in the transverse direction (Y-direction), while Specimen 2 was cut from the longitudinal direction of the deposit. The FSed coating strength was found to be 14% higher in the longitudinal direction compared to the transverse direction.

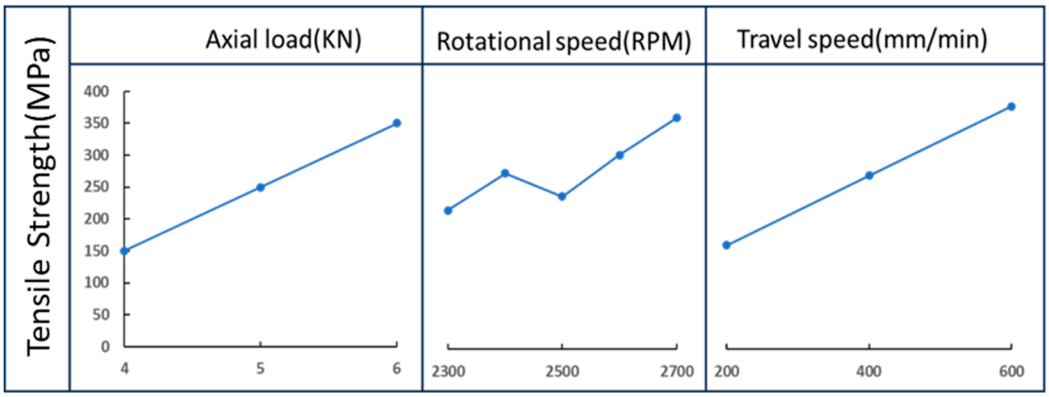


Figure 13. Influence of process parameters on ultimate tensile strength (UTS) of the FSed coating.

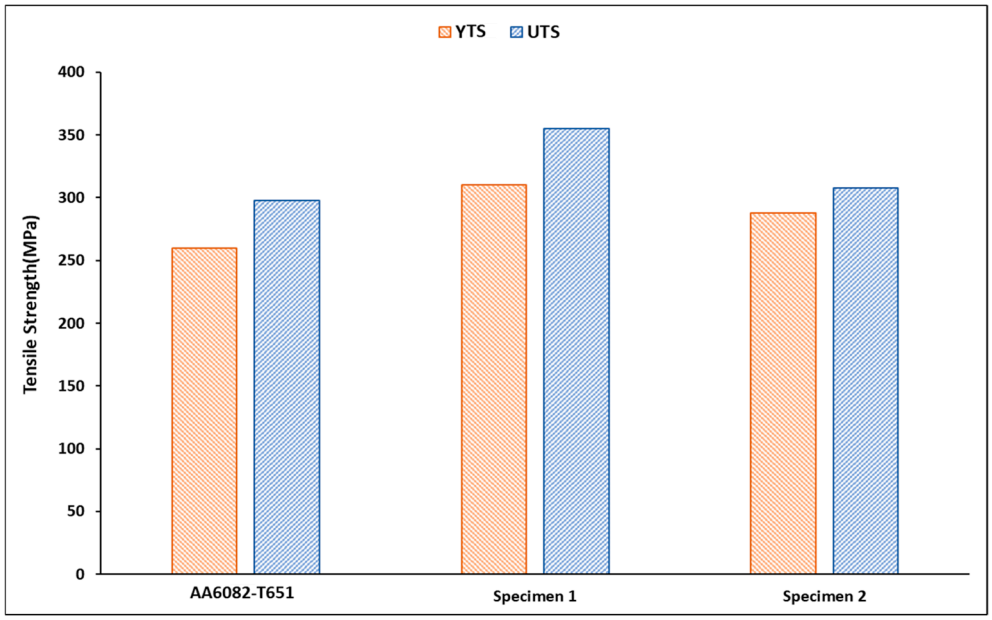


Figure 14. Tensile testing of AA6082-coated EN14B steel specimen using FS process.

The heat treatment of the FSed samples resulted in a 13.03% increase in the average UTS and a 9.79% increase in yield tensile strength (YTS). However, a decrease of 6.87% in elongation was also observed. It can be inferred that the tensile strength is directly proportional to the friction pressure, rotational speed, and travel speed.

3.5. Correlation in Process Parameters and Thermal Parameters

The friction stir welding (FSW) machine was operated in force-controlled mode, as shown in Figure 1. The variation of axial thrust and generated torque from the experiments are shown in Figure 15a,b, respectively. A sudden rise in load marks at the beginning of the deposition phase. In the FS process, the dwell phase refers to the period during which the consumable rod is held stationary against the substrate without forward movement. During this phase, frictional heat is generated due to the relative motion between the rotating rod and the substrate, which softens the consumable material at the contact interface. Once sufficient heat is generated to soften the consumable rod, the deposition phase begins. A sudden drop in load may indicate improper heat generation or potential tool wear, whereas a continuous stable load profile throughout the deposition phase reflects good process control and repeatability of the weld quality. During the dwell phase (when no axial force is applied to the consumable rod), the consumable material begins to plasticize, and the dry friction transitions into lubricated friction. The flow of plasticized material reaches a steady state when the temperature reaches its maximum range, at which point the frictional torque decreases. This phase is termed the adiabatic phase [1,31].

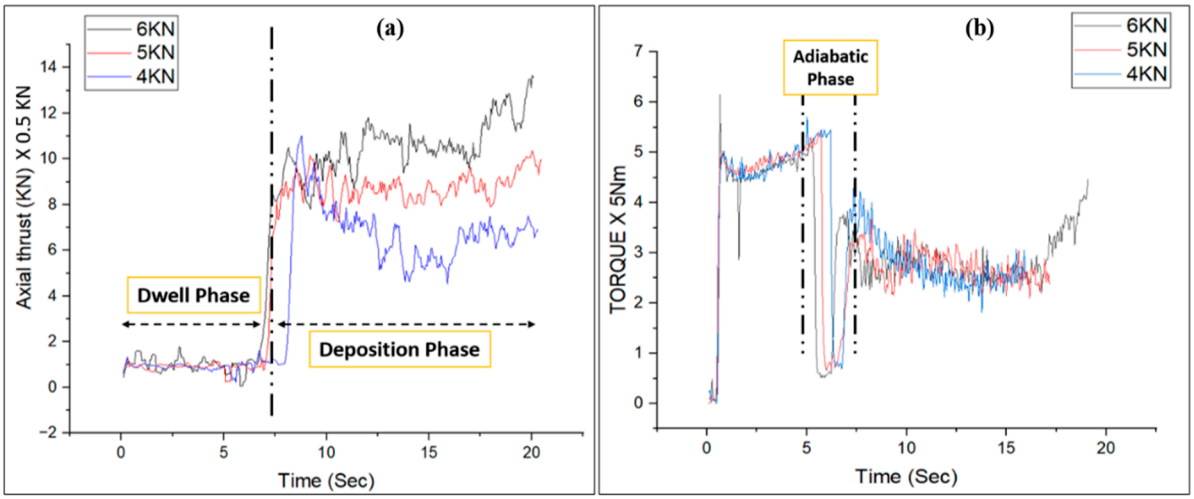


Figure 15. Variation of (**a**) Load and, (**b**) torque profile vs. processing time obtained from FSW machine data.

However, it is important to note that FSW and FS are distinct processes, particularly in terms of tool geometry, depth of penetration, and material flow characteristics. The equation proposed by Kar et al. [32] was employed in this study to provide a first approximation of the peak temperature, primarily for comparing heat input across different processing conditions (i.e., rotational speed, axial load, and traverse speed) rather than for determining the absolute peak temperature. While the depth of penetration and tool design in FS play a critical role in temperature prediction, the FS process involves a consumable rod that deposits material onto the substrate, and the depth of penetration differs significantly. Therefore, the use of the Mishra et al. equation in this study serves as a comparative tool for assessing heat input rather than as a precise temperature predictor.

Process parameter variations have a direct effect on thermal parameters, such as heat input and process temperature, which are critical to the quality of the deposit. The process

temperature, which influences the deposit's mechanical properties and microstructure, is directly related to the heat input during FS processing. The torque values measured by the machine can be used to estimate the amount of heat and power input for welding [31,33]. Table 6 presents the calculated values of heat input for samples deposited under different processing parameters. Samples denoted with "*" in Table 6 are with good or intermittent bonding quality. Additionally, Equation (3) is used to estimate the approximate peak temperature during the process for all parameters [34]; the peak temperatures for all parameters are shown in Table 6.

Table 6. Calculated values of heat input and peak temperature during the FS process.

S.No.	F	N	V	Avg. Torque (N-m)	Power (W)	Heat Input (kJ/mm)	Peak Temperature (°C)	Discussion
S5 *	5(0)	2500(0)	600(+1)	27.5	7195.8	0.7	413	Continuous but non-uniform bonding strength
S6 *	5(0)	2700(+1)	200(−1)	23.0	6499.8	1.9	434	Thick intermetallic
S7	6(+1)	2300(−1)	600(+1)	24.9	5994.2	0.6	348	Discontinuous bonding
S8 *	6(+1)	2500(0)	200(−1)	22.5	5887.5	1.8	366	Thick intermetallic
S9 *	6(+1)	2700(+1)	400(0)	26.5	7488.9	1.1	422	Continuous and uniform bonding strength

"*" corresponding to good or intermittend bond quality.

Higher heat input promotes deeper melting, which facilitates interdiffusion and results in stronger and more durable bonds. However, overheating of aluminum can lead to oxidation, diminishing weld quality. Excessive heat can also induce microstructural changes, making the coating brittle. Similarly, higher peak temperatures promote interdiffusion and stronger bonding, but the bond strength may be compromised by brittle intermetallic phases that form at the interface due to excessive temperatures.

A balanced approach, focusing on both heat input and peak temperature control, is essential for achieving optimal bonding in FS. From Table 6, it can be noted that samples S6 and S8, which exhibit higher heat input, result in thicker coatings, while Sample S7 yields a spot-wise coating due to insufficient temperature during the FS process. Sample S5 produces more flash mass due to a high temperature but a weaker bond because of lower heat input; annealing can improve the bonding strength and hardness of both S5 and S9 coatings [35]. Optimizing heat input, process temperature, and axial load is crucial for achieving higher bonding strength in FS coatings.

During the friction surfacing deposition of aluminum 6063 over IS 2062 low-carbon steel with various electrodes, the process temperature was observed to be in the range of 400–450 °C [7]. Based on the intermetallic compound (IMC) formation data presented in Table 5, the stoichiometry of the coated samples shown in Figures 8 and 9, and the process temperature data in Table 6, it can be concluded that Al-rich IMCs form at around 430 °C, and then transition into Fe-rich IMCs following post-heat treatment at 550 °C for 48 h, enhancing the overall mechanical properties of the FSed coated samples [36].

3.6. Comparative Analysis with Existing Studies

In our study, a significant advance in the field of FS, using optimized FS parameters and a post-heat-treatment strategy for AA6082-T651 deposited on EN14B steel to improve coating integrity, microstructural, and mechanical properties, is discussed.

Optimization of processing parameters plays a significant role in the improvement of the structural integrity, bonding quality, and mechanical performance of any dissimilar structure and coating. The present investigation reveals that an axial load of 6 kN, consumable tool rotation speed of 2700 rpm, and travel speed of 400 mm/min, resulted in the highest surfacing quality and tensile strength. This result aligns with the study performed by Janakiraman et al. [15], which showed the importance of optimizing axial load in achieving better bond strength in the FS coating of AA6063 aluminum alloy over AISI316 stainless steel at optimal parameters of 5 KN, 2400 rpm, 150 mm/min, and a tool diameter of 20 mm; the coating thickness was 1.96 mm and coating width 18.12 while, in the present work, the coating thickness achieved is 0.90 ± 0.28 mm and the coating width is 34 ± 0.15 mm at the optimal parameters of 6 KN, 2700 rpm, 400 mm/min, and a tool diameter of 20 mm [37]. Higher load and higher rotational speed serve better coating integrity in the physical characteristics of the coatings [38]; this study aligns with the present work as well. In the present investigation, peak temperature during the FS process was estimated as 422 °C, which corroborates the results of the investigation on aluminum–steel FS deposition [5]. Those results exhibited a peak temperature of 421 °C. Such a close correlation between the research findings confirms that the precise control of heat input and processing parameters improves mechanical properties, primarily by minimizing defects and improving coating integrity with substate materials [7,15]. The temperature profile in the friction deposition of A6063 aluminum alloy onto EN24 carbon steel was experimentally studied by Sahoo and Mohanty [35] and is comparatively similar to the process temperature calculated in this study.

The post-heat-treatment strategy used in the present investigation further affects the quality of the interface and improves the mechanical properties by controlling the microstructure and IMC compounds. A notable transition from Al-rich IMCs to Fe-rich IMCs was observed after annealing at 550 °C for 48 h. Such a transition and formation of Fe_3Al after 48 h of annealing at 550 °C results in a significantly enhanced bonding strength [4,16]. This result is consistent with prior research on FS by Reddy et al. [2] and Li et al. [6], who demonstrated that Fe_3Al is a critical IMC phase in aluminum–steel diffusion bonding. However, unlike that of Sahoo et al. [8], who applied heat treatment before FS, this study demonstrated that post-HT leads to superior bonding strength, hardness, and diffusion efficiency. The hardness at the Al–steel interface increased significantly after heat treatment, which aligns with the findings of Manesh et al. [17] and Zhang et al. [19], who demonstrated that Fe-rich IMCs enhance bonding strength and structural integrity. In addition, the present investigation also showes that grain size and the IMC phase can be controlled using a heat treatment strategy. The coating grains are highly refined and equiaxed due to the continuous dynamic recrystallization (CDRX) in FS. Also, the aluminum grains were significantly diminished after FS due to the CDRX, resulting in a smaller average grain diameter of 4.45 μm, compared with that of the Al rod, which was 36.35 μm [39]. The same phenomena occur in the present work during the FS of AA6082 T-651 onto EN14B, where grains of aluminum were reduced to 9.09 ± 0.45 μm and, after heat treatment, grains were reduced to 6.09 ± 0.25 μm.

Furthermore, post-heat treatment improved the diffusion and mechanical properties of the FSed coating [17,20]. Heat input, in the present study, was quantified as 1.1 kJ/mm in the case of optimized bonding and IMC formation. This observation aligns with the work of Govardhan et al. [13], who reported that optimized heat input is a critical factor in enhancing deposition efficiency. With low energy input, flash formation at the consumable rod can be controlled using appropriate process parameters during friction surfacing. The process parameters influenced the physical dimensions of the AA6063 aluminum alloy coating on mild steel in friction surfacing [40]. This approach can be used and compared

to that of Kumar Sahoo et al. [8], who employed forced convection and inductive heating to control oxidation and intermetallic evolution. The results illustrate that controlled heat input plays a pivotal role in achieving optimal bonding strength. Samples subjected to lower heat input exhibited discontinuous bonding, whereas excessive heat input resulted in increased flash formation and microstructural coarsening. Heat input conditions affect the microstructure evolution, elemental diffusion, phase formation, and bond quality due to the simultaneous impact of thermal history, mechanical mixing, and strain-induced diffusion, as reported by Kar et al. [41,42].

The present study advances the science by demonstrating the effectiveness of annealing in refining grain structure and improving mechanical performance. The systematic phase analysis of intermetallic evolution and the corresponding microstructure characterization further supports the hypothesis that prolonged heat treatment enhances atomic diffusion and bond strength. The formation of Fe_3Al and $Al_{0.5}Cr_{0.5}Fe_1$ compounds after 48 h of annealing suggests that extended heat treatment accelerates diffusion-driven phase transformations, leading to superior mechanical performance. The integration and correlation of experimental process optimization using a statistical method (Taguchi orthogonal array) with microstructural characterization and mechanical property evolution provides a comprehensive understanding of the interplay between process conditions, IMC evolution, and mechanical properties and, therefore, contributes valuable insights to the field of solid-state coatings of dissimilar materials.

4. Conclusions

In this study, the deposition of AA6082 T-651 on an EN14B steel plate was successfully achieved using the friction surfacing (FS) process. The effects of process optimization and post-heat treatment on the microstructural and mechanical properties of the FSed coatings were investigated. The following conclusions were drawn:

(a) The analysis of process and thermal parameters reveals that, once the FS process achieves the desired level of heat input and the consumable material reaches its peak temperature, axial load plays a pivotal role in ensuring optimal mechanical interlocking throughout the deposition. Post-heat treatment of the FSed coated samples promotes atomic diffusion bonding, resulting in enhanced bonding strength.

(b) Acceptable FSed coatings were obtained at an axial load of 5–6 kN and a rotational speed of 2500–2700 RPM. The process temperature during the friction surfacing deposition of AA6082 T-651 on an EN14B steel plate ranged from 330 °C to 440 °C.

(c) Annealing for 48 h at 550 °C resulted in effective interdiffusion, converting Al-rich intermetallic compounds (IMCs) into Fe-rich IMCs in Sample S9 (HT), with the formation of Fe_3Al compounds and an improvement in the mechanical properties of the coating.

(d) The microhardness at the Al–steel interface was 138 HV0.1 in Sample S9 (HT) (48 h post-heat treatment) and 132 HV0.1 in Sample S9 (36 h post-heat treatment). Additionally, the tensile strength at the Al–steel interface in FSed coated samples was found to be greater in the longitudinal direction of the deposit compared to the transverse direction.

(e) These findings suggest that the optimization of friction surfacing parameters and the implementation of post-heat treatment significantly enhance the microstructural and mechanical properties of AA6082 T-651 coatings on EN14B steel plates.

(f) The integration of experimental process optimization with microstructural and mechanical characterization provides a comprehensive understanding of the interplay between process conditions, IMC evolution, and mechanical properties, contributing valuable insights to the field of solid-state coatings.

Author Contributions: Conceptualization, N.K.S.; methodology, H.J., N.K.S. and A.K.; formal analysis, H.J. and A.K.; investigation, H.J. and A.K.; resources, N.K.S. and A.K.; Writing—original draft, H.J. and A.K.; Writing—review & editing, H.J. and A.K.; Funding acquisition, N.K.S. and A.K. All authors have read and agreed to the published version of the manuscript.

Funding: This research received no external funding.

Data Availability Statement: Data are contained within the article.

Acknowledgments: The authors would like to thank the Department of Mechanical Engineering and the foundry lab of IISc, Bengaluru, as well as the central workshop and the Central Research Facility (CRF) of IIT (ISM), Dhanbad, for their support in this research.

Conflicts of Interest: The authors declare no conflicts of interest that could have influenced the findings or interpretations presented in this paper.

References

1. Gandra, J.; Krohn, H.; Miranda, R.M.; Vilaça, P.; Quintino, L.; dos Santos, J.F. Friction Surfacing—A Review. *J. Mater. Process. Technol.* **2014**, *214*, 1062–1093. [CrossRef]
2. Reddy, G.M.; Prasad, K.S.; Rao, K.S.; Mohandas, T. Friction Surfacing of Titanium Alloy with Aluminium Metal Matrix Composite. *Surf. Eng.* **2011**, *27*, 92–98. [CrossRef]
3. Seidi, E.; Miller, S.F.; Carlson, B.E. Friction Surfacing Deposition by Consumable Tools. *J. Manuf. Sci. Eng.* **2021**, *143*, 120801. [CrossRef]
4. Yu, M.; Zhao, H.; Zhang, Z.; Zhou, L.; Song, X. Friction Surfacing Assisted Refilled Friction Stir Spot Welding of AA6061 Alloy and Q235 Steel. *J. Manuf. Process.* **2022**, *77*, 1–12. [CrossRef]
5. Badheka, K.; Badheka, V. Friction Surfacing of Aluminium on Steel: An Experimental Approach. *Mater. Today Proc.* **2017**, *4*, 9937–9941. [CrossRef]
6. Li, H.; Qin, W.; Galloway, A.; Toumpis, A. Friction Surfacing of Aluminium Alloy 5083 on DH36 Steel Plate. *Metals* **2019**, *9*, 479. [CrossRef]
7. Sahoo, D.K.; Guna, P.; Deepan, S. Performance Analysis on Deposition of Aluminium 6063 over En8 Medium Carbon Steel by Friction Surfacing. *Mater. Today Proc.* **2022**, *64*, 116–123. [CrossRef]
8. Kumar Sahoo, D.; Babu Chaudhary, S.; Neupane, N. Study on Mechanical Behaviour of Aluminium 6063 Deposition on EN8 Carbon Steel by Forced Convection Friction Surfacing Process. *Mater. Today Proc.* **2023**. [CrossRef]
9. Sahoo, D.K.; Pradeep, A.M.V.; Mohanty, B.S.; Jaswanth, A. Influence of Inductive Heating on Coating Geometry during Deposition of AISI 316 Stainless Steel over EN8 Carbon Steel Using Friction Surfacing Process. *Mater. Today Proc.* **2020**, *27*, 1641–1650. [CrossRef]
10. Cyril Joseph Daniel, S.; Damodaram, R.; Karthik, G.M.; Lakshmana Rao, B. Friction Surfaced Alloy 718 Deposits: Effect of Process Parameters on Coating Performance. *J. Mater. Eng. Perform* **2022**, *31*, 4119–4132. [CrossRef]
11. Fitseva, V.; Hanke, S.; Dos Santos, J.F. Influence of Rotational Speed on Process Characteristics in Friction Surfacing of Ti-6Al-4V. *Mater. Manuf. Process.* **2017**, *32*, 557–563. [CrossRef]
12. Stegmueller, M.J.R.; Grant, R.J.; Schindele, P. Quantification of the Interfacial Roughness When Coating Stainless Steel onto Aluminium by Friction Surfacing. *Surf. Coat. Technol.* **2019**, *375*, 22–33. [CrossRef]
13. Govardhan, D.; Kumar, A.C.S.; Murti, K.G.K.; Madhusudhan Reddy, G. Characterization of Austenitic Stainless Steel Friction Surfaced Deposit over Low Carbon Steel. *Mater. Des. (1980–2015)* **2012**, *36*, 206–214. [CrossRef]
14. Pereira, D.; Gandra, J.; Pamies-Teixeira, J.; Miranda, R.M.; Vilaça, P. Wear Behaviour of Steel Coatings Produced by Friction Surfacing. *J. Mater. Process. Technol.* **2014**, *214*, 2858–2868. [CrossRef]
15. Janakiraman, S.; Bhat, K.U. Formation of Composite Surface during Friction Surfacing of Steel with Aluminium. *Adv. Tribol.* **2012**, *2012*, 614278. [CrossRef]
16. Yang, X.; Weng, H.; Tang, C. Interfacial Bonding Mechanism Ofaluminium and Steel Composites. *Adv. Compos. Lett.* **2018**, *27*, 096369351802700203. [CrossRef]
17. Danesh Manesh, H.; Karimi Taheri, A. The Effect of Annealing Treatment on Mechanical Properties of Aluminum Clad Steel Sheet. *Mater. Des.* **2003**, *24*, 617–622. [CrossRef]
18. Martins, N.; Silva, A.P.; Cordeiro Da Silva, G.; Dos Santos, Í.B.; Santos, C.E.D.; Troysi, F.; Brito, P. Characterization of Iron Aluminide Diffusion Coatings Obtained after Friction Surfacing. *Metals* **2023**, *13*, 461. [CrossRef]
19. Zhang, T.; Wang, K.; Qiao, K.; Wu, B.; Liu, Q.; Han, P.; Wang, W.; Wang, Y.; Hao, Z.; Zheng, P. Evolution mechanism of intermetallic compounds and the mechanical properties of dissimilar friction stir welded QP980 steel and 6061 aluminum alloy. *Mater. Charact.* **2023**, *202*, 113033. [CrossRef]

20. Jiang, B.; Cai, Q.; Tao, H.; Zhang, W.; Zhang, H. The effect of heat treatment on the microstructure and mechanical properties of 6082 aluminum alloy manufactured by friction stir additive. *Mater. Charact.* **2025**, *220*, 114680. [CrossRef]
21. Beygi, R.; Galvão, I.; Akhavan-Safar, A.; Pouraliakbar, H.; Fallah, V.; da Silva, L.F. Effect of alloying elements on intermetallic formation during friction stir welding of dissimilar metals: A critical review on aluminum/steel. *Metals* **2023**, *13*, 768. [CrossRef]
22. Bergh, T.; Arbo, S.M.; Hagen, A.B.; Blindheim, J.; Friis, J.; Khalid, M.Z.; Ringdalen, I.G.; Holmestad, R.; Westermann, I.; Vullum, P.E. On intermetallic phases formed during interdiffusion between aluminium alloys and stainless steel. *Intermetallics* **2022**, *142*, 107443. [CrossRef]
23. Vitanov, V.I.; Javaid, N.; Stephenson, D.J. Application of response surface methodology for the optimisation of micro friction surfacing process. *Surf. Coat. Technol.* **2010**, *204*, 3501–3508. [CrossRef]
24. Vitanov, V.I.; Voutchkov, I.I. Process parameters selection for friction surfacing applications using intelligent decision support. *J. Mater. Process. Technol.* **2005**, *159*, 27–32. [CrossRef]
25. Haghshenas, M.; Abdel-Gwad, A.; Omran, A.M.; Gökçe, B.; Sahraeinejad, S.; Gerlich, A.P. Friction Stir Weld Assisted Diffusion Bonding of 5754 Aluminum Alloy to Coated High Strength Steels. *Mater. Des.* **2014**, *55*, 442–449. [CrossRef]
26. Kar, A.; Kailas, S.V.; Suwas, S. Effect of Zinc Interlayer in Microstructure Evolution and Mechanical Properties in Dissimilar Friction Stir Welding of Aluminum to Titanium. *J. Mater. Eng. Perform.* **2018**, *27*, 6016–6026. [CrossRef]
27. Abbasi, M.; Dehghani, M.; Guim, H.U.; Kim, D.I. Investigation of Fe-rich fragments in aluminum-steel friction stir welds via simultaneous Transmission Kikuchi Diffraction and EDS. *Acta Mater.* **2016**, *117*, 262–269. [CrossRef]
28. Kar, A.; Vicharapu, B.; Morisada, Y.; Fujii, H. Elucidation of Interfacial Microstructure and Properties in Friction Stir Lap Welding of Aluminium Alloy and Mild Steel. *Mater. Charact.* **2020**, *168*, 110572. [CrossRef]
29. Gupta, R.; Thakur, L. Development of an AA 7075 Wear-Resistant Coating on AA 6082 via Friction Surfacing: Optimization and Characterization. *J. Mater. Eng Perform* **2023**, *32*, 10311–10325. [CrossRef]
30. *ASTM. Standard E8E8M-16a*; Test Methods for Tension Testing of Metallic Materials. ASTM International: West Conshohocken, PA, USA, 2016.
31. Bararpour, S.M.; Jamshidi Aval, H.; Jamaati, R. Modeling and Experimental Investigation on Friction Surfacing of Aluminum Alloys. *J. Alloys Compd.* **2019**, *805*, 57–68. [CrossRef]
32. Kar, A.; Curtis, T.; Jasthi, B.K.; Lein, W.; McClelland, Z.; Crawford, G. Mechanism of Joint Formation in Dissimilar Friction Stir Welding of Aluminum to Steel. In *Friction Stir Welding and Processing XII*; Hovanski, Y., Sato, Y., Upadhyay, P., Naumov, A.A., Kumar, N., Eds.; Springer: Cham, Switzerland, 2023; pp. 237–245.
33. Colligan, K.J.; Mishra, R.S. A Conceptual Model for the Process Variables Related to Heat Generation in Friction Stir Welding of Aluminum. *Scr. Mater.* **2008**, *58*, 327–331. [CrossRef]
34. Mishra, R.S.; Ma, Z.Y. Friction Stir Welding and Processing. *Mater. Sci. Eng. R Rep.* **2005**, *50*, 1–78. [CrossRef]
35. Sahoo, D.K.; Mohanty, B.S. Evaluation of bond strength on deposition of aluminium 6063 alloy over EN24 medium carbon steel by friction surfacing using different mechtrode diameter. *e-J. Surf. Sci. Nanotechnol.* **2019**, *17*, 83–94. [CrossRef]
36. Geng, P.; Morimura, M.; Ma, H.; Ma, Y.; Ma, N.; Liu, H.; Aoki, Y.; Fujii, H.; Qin, G. Elucidation of Intermetallic Compounds and Mechanical Properties of Dissimilar Friction Stir Lap Welded 5052 Al Alloy and DP590 Steel. *J. Alloys Compd.* **2022**, *906*, 164381. [CrossRef]
37. Sahoo, D.K.; Chari, A.N.; Reddy, A.S. Optimization & characterization of friction surfaced coatings of AA6063 aluminium alloy over AISI316 stainless steel substrate. *Mater. Today Proc.* **2020**, *23*, 565–572.
38. Kumar, B.V.; Reddy, G.M.; Mohandas, T. Influence of process parameters on physical dimensions of AA6063 aluminium alloy coating on mild steel in friction surfacing. *Def. Technol.* **2015**, *11*, 275–281. [CrossRef]
39. Yu, M.; Zhang, Z.; Zhao, H.; Zhou, L.; Song, X. Microstructure and corrosion behavior of the ultra-fine grained aluminum coating fabricated by friction surfacing. *Mater. Lett.* **2019**, *250*, 174–177. [CrossRef]
40. Fitseva, V.; Krohn, H.; Hanke, S.; Dos Santos, J.F. Friction surfacing of Ti–6Al–4V: Process characteristics and deposition behaviour at various rotational speeds. *Surf. Coat. Technol.* **2015**, *278*, 56–63. [CrossRef]
41. Kar, A.; Suwas, S.; Kailas, S.V. Microstructural Modification and High-Temperature Grain Stability of Aluminum in an Aluminum-Titanium Friction Stir Weld with Zinc Interlayer. *JOM* **2019**, *71*, 444–451. [CrossRef]
42. Kar, A.; Kailas, S.V.; Suwas, S. Effect of Mechanical Mixing in Dissimilar Friction Stir Welding of Aluminum to Titanium with Zinc Interlayer. *Trans. Indian Inst. Met.* **2019**, *72*, 1533–1536. [CrossRef]

Disclaimer/Publisher's Note: The statements, opinions and data contained in all publications are solely those of the individual author(s) and contributor(s) and not of MDPI and/or the editor(s). MDPI and/or the editor(s) disclaim responsibility for any injury to people or property resulting from any ideas, methods, instructions or products referred to in the content.